NASA Contractor Report 189743
ICASE Report No. 92–69

ICASE

ESTIMATING UNCERTAINTY IN COMPUTATIONS OF TWO-DIMENSIONAL SEPARATED FLOWS

A. O. Demuren
R. V. Wilson

NASA Contract Nos. NAS1–18605 and NAS1–19480
December 1992

Institute for Computer Applications in Science and Engineering
NASA Langley Research Center
Hampton, Virginia 23681–0001

Operated by the Universities Space Research Association

National Aeronautics and
Space Administration
Langley Research Center
Hampton, Virginia 23665-5225

ESTIMATING UNCERTAINTY IN COMPUTATIONS OF TWO-DIMENSIONAL SEPARATED FLOWS

A. O. Demuren[1] *and R. V. Wilson*
Department of Mechanical Engineering and Mechanics
Old Dominion University
Norfolk, VA 23529

ABSTRACT

The present paper investigates sources of uncertainties in two-dimensional flow computations and presents methods for estimating them. Two sample problems are used for illustration. The following categories are explored in detail: i.) Uncertainty due to truncation error in numerical schemes; ii.) Uncertainty due to discretization error; iii.) Uncertainty due to outflow boundary conditions; iv.) Uncertainty due to incomplete iterative convergence; v.) Uncertainty due to computational grid aspect ratio. The error estimates are based on requirements for internal consistencies in computed results. Therefore, they provide better judgement of the numerical solution integrity than comparisons to experimental data or "benchmark" solutions whose reliability may sometimes be questionable. Ideally, both approaches should be employed. New results are presented on the optimum grid-cell aspect ratio for computational accuracy and efficiency.

[1]Research was supported by the National Aeronautics and Space Administration under NASA Contract Nos. NAS1-18605 and NAS1-19480 while the first author was in residence at the Institute for Computer Applications in Science and Engineering (ICASE), NASA Langley Research Center, Hampton, VA 23681-0001.

1 INTRODUCTION

The rapid development of computers over the past three decades has encouraged the development of computational fluid dynamics to such an extent that it has become a viable analytical tool in the solution or design process in several engineering and environmental applications. As the investigated flow situations have become more complicated, the need for techniques for evaluating sources and magnitudes of uncertainties in computed results have grown. Unfortunately, too little attention has been paid to this subject in the literature. Most work is done by numerical analysts in highly idealized situations. The dilemma facing the computational fluid dynamists is that the logical test of the accuracy of a numerical method is to compare computed results to exact solutions. But these can rarely be found for practically interesting problems. So one resorts to comparing computed results to other numerical solutions, sometimes called "benchmark" solutions, or experimental data. Such a comparison, may be diagnostic, but would usually be inconclusive since the latter may contain unknown errors. Therefore, there is a need for techniques which allow quantitative estimation of various uncertainties in the numerical solution in a systematic manner.

Ferziger (1989) proposed some methods suitable for the estimation and reduction of numerical errors resulting from inadequate grid resolution or incomplete convergence of the iterative scheme. The former is based on the Richardson extrapolation method originally proposed by Richardson (1911) and Richardson and Gaunt (1927). This method has been used in a wide range of applications to improve numerical solutions or to estimate errors in numerical solutions. Churchill et al. (1981) and de Vahl Davis (1983) applied the method to estimate zero-grid-size solution in natural convection problems. Applications to aerodynamic flows are reported by Dang et al. (1989) and Zing (1991), amongst others. The common result is that the Richardson extrapolation method is reliable only when the numerical solutions on the different grids used in the procedure are smooth and display similar characteristics, which presupposes that the grids should be sufficiently fine to resolve all flow features. The method for removing the uncertainty of incomplete convergence of the iterative scheme is to base the convergence criterion not on the change in computed results between iterations, as is common in practice, but on an estimate of the solution error constructed from both the change and its rate of change. This method requires little additional effort but has not yet found wide use.

In the present paper, we investigate a wider range of sources of uncertainty in numerical computations of separated flows. Possible errors resulting from each source are estimated and methods for eliminating or minimizing them are explored. Two model problems were used in the investigation. The first is the steady, two-dimensional laminar flow over a backward facing step, and the second is a steady, two-dimensional stratified laminar flow over a backward facing step. The Reynolds number in both flow problems was at the high end of the laminar flow range (equal to 400 based on the mean flow velocity and the channel height upstream of the step). The flow configurations and the boundary conditions are illustrated in Figures 1 and 2. "Benchmark" solutions for these problems have been developed by Gartling (1990) for problem 1 and Leone (1990) for problem 2. Streamlines of these are shown in Figure 3. Our results are also compared to these solutions, as estimates of the exact solutions but with the reservations mentioned above. It should be noted that in both cases, the original authors used the Richardson extrapolation method as outlined in section 4 of the present paper to estimate some of the uncertainties in their results, so they may be considered reliable.

2 NUMERICAL METHOD

The equations governing the steady, two-dimensional, incompressible flow and heat transfer can be written in dimensionless variables as:

$$\frac{\partial u}{\partial x}+\frac{\partial v}{\partial y}=0 \tag{1}$$

$$u\frac{\partial u}{\partial x}+v\frac{\partial u}{\partial y}=-\frac{\partial p}{\partial x}+\frac{1}{Re}\left(\frac{\partial^2 u}{\partial x^2}+\frac{\partial^2 u}{\partial y^2}\right) \tag{2}$$

$$u\frac{\partial v}{\partial x}+v\frac{\partial v}{\partial y}=-\frac{\partial p}{\partial y}+\frac{1}{Re}\left(\frac{\partial^2 v}{\partial x^2}+\frac{\partial^2 v}{\partial y^2}\right)+\frac{T}{Fr} \tag{3}$$

$$u\frac{\partial T}{\partial x}+v\frac{\partial T}{\partial y}=\frac{1}{RePr}\left(\frac{\partial^2 T}{\partial x^2}+\frac{\partial^2 T}{\partial y^2}\right) \tag{4}$$

where Re, Pr, and Fr are respectively, the Reynolds number, Prandtl number and the densimetric Froude number.

The equations are solved with modified versions of the popular TEACH computer code, which is based on the SIMPLE algorithm of Patankar and Spalding (1972). In the original TEACH code, the differential equations were discretized using numerical approximations to derivatives over a staggered computational grid. Convection terms were approximated with a hybrid of central and first-order upwind differences, depending on whether the cell Peclet number was less or greater than two, and diffusion and other terms were approximated with central differences. It turns out that in high Reynolds number computations on typical grids, the hybrid scheme mostly degenerates to a first-order upwind scheme which introduces "artificial diffusion" into the solution. Effect of the discretization of the convection terms is considered in section 3, where the hybrid method is compared with other higher-order difference methods.

The boundary conditions for case 1 and 2 are shown in Figure 1 and 2. For the inflow, a parabolic profile is prescribed such that $u(y) = 12y - 24y^2$ for $x = 0, 0 < y < 1/2$. At solid surfaces, the typical "no slip" condition of zero velocity is applied. For test case 2, additional boundary conditions are necessary for the temperature equation. The non-dimensional temperature of the top wall is set to 1, while that of the bottom wall is set to 0. A linear temperature profile is prescribed at the inlet plane with $T = 0$ at the step corner, and $T = 1$ at the top wall, i.e. $T(y) = 2y$ $(x = 0, 0 < y < 1/2)$. The streamwise temperature derivative is set to zero on the step side wall $(x = 0, -1/2 < y < 0)$. The boundary condition at the outflow plane will be described in section 5.

In sections 3 and 6, uniform grid spacing is used with 258 points in the streamwise direction and 34 points in the cross stream direction. An x domain length of 10 units is used. For the results of section 4 and 5, nonuniform grid spacings are used. Section 5 investigates the effect of the location of the outflow boundary by using four x domain lengths. Grid 1 is defined using a streamwise domain length of 30 units and 480 streamwise points. Grids 2-4 are simple truncations of grid 1. The domain lengths for grids 2-4 are 15, 10, and 7 streamwise units giving 412, 372, and 337 streamwise points, respectively. In the cross channel direction, 41 points are used for grids 1-4. The streamwise spacing of the base grid 1 is expanded geometrically by a factor of 1.01 going

from 0 to 30 units downstream, while the vertical grid spacing is expanded by a factor of 1.05 moving from the top and bottom walls towards the center line of the channel. Convergence for the model problems was typically achieved in about 4000 iterations.

3 TRUNCATION ERROR IN NUMERICAL SCHEMES

3.1 Description of the numerical schemes

Truncation error in a numerical scheme may result from errors in approximating the convection or diffusion terms, but in high Reynolds number flows convection usually dominates diffusion so more attention needs to be placed on the former. Further, stability or algorithmic considerations may place restrictions on the form of the convective terms, so the analysis of truncation errors in the numerical schemes concentrates on the approximation for the convection terms. The diffusion terms are simply approximated with central differences.

Four differencing schemes are applied to the two model problems. The differencing schemes are the hybrid, central, second-order upwind (2nd OU), and third-order upwind (3rd OU). On discretizing the governing equations (1), (2), (3) and (4) over a typical control volume, the four schemes lead to algebraic equations with the general form:

$$A_P\phi_P = A_E\phi_E + A_W\phi_W + A_N\phi_N + A_S\phi_S + A_{EE}\phi_{EE} + A_{WW}\phi_{WW} + A_{NN}\phi_{NN} + A_{SS}\phi_{SS} + S_u + B \quad (5)$$

where ϕ is any field property (velocity or temperature), S_u is the source term, (pressure gradient or additional viscous terms), the A's are the convection/diffusion coefficients, and B is the fluid body force, where applicable.

A typical control volume is shown in Figure 4 along with the neighboring points. The points *e*, *n*, *w*, and *s* refer to values at the east, north, west, and south cell faces, respectively. The points *E*, *W*, *N*, and *S* refer to grid points to the east, north, west, and south of the cell center, respectively. The points *EE*, *WW*, *NN*, and *SS* are grid points located to the east, north, west, and south, two points away from the cell center, respectively.

The convection through the cell faces is defined as:

$$F_e \equiv u_e \Delta y \quad (6)$$

$$F_w \equiv u_w \Delta y \quad (7)$$

$$F_n \equiv v_n \Delta x \quad (8)$$

$$F_s \equiv v_s \Delta x \quad (9)$$

The diffusion at the cell faces is defined as:

$$D_e \equiv \frac{\Gamma_e}{\Delta x} \Delta y \quad (10)$$

$$D_w \equiv \frac{\Gamma_w}{\Delta x}\Delta y \tag{11}$$

$$D_n \equiv \frac{\Gamma_n}{\Delta y}\Delta x \tag{12}$$

$$D_s \equiv \frac{\Gamma_s}{\Delta y}\Delta x \tag{13}$$

where Γ is the diffusion coefficient of the field property ϕ. It is equal to $(1/Re)$ for the momentum equation and $(1/RePr)$ for the temperature equation. The ratio F/D is the Peclet number on the grid-cell face. The convection velocity through the west cell face is defined as:

$$u_w \equiv \frac{1}{2}(u_P + u_W)$$

The A coefficients in equation (5) are determined by the numerical scheme to be used.

3.1.1 Hybrid scheme

The coefficients for the hybrid scheme have the following form:

$$A_E = \max\left[0, D_e - \frac{1}{2}|F_e|\right] + \max\left[-F_e, 0\right] \tag{14}$$

$$A_W = \max\left[0, D_w - \frac{1}{2}|F_w|\right] + \max\left[F_w, 0\right] \tag{15}$$

$$A_N = \max\left[0, D_n - \frac{1}{2}|F_n|\right] + \max\left[-F_n, 0\right] \tag{16}$$

$$A_S = \max\left[0, D_s - \frac{1}{2}|F_s|\right] + \max\left[F_s, 0\right] \tag{17}$$

$$A_{EE} = A_{WW} = A_{NN} = A_{SS} = 0 \tag{18}$$

$$A_P = \sum A_i \tag{19}$$

where the sum for A_p is taken over the A coefficients, and $|\ |$ represents the absolute value.

A truncation of the hybrid scheme gives the first-order upwind (1st OU) scheme, which is much less accurate. For this scheme, the coefficients are calculated from only the second term of the right hand side of equations (14)-(17). If the cell Peclet number was greater than two in all regions of the flow, this scheme would be used throughout, but such a condition cannot be true in a separated flow.

3.1.2 Central, second-order upwind, and third-order upwind difference schemes

The coefficients for the higher-order schemes have the following general form:

$$A_E = (D_e - \frac{F_e}{2}) + (f_1 \max [F_e, 0] + f_1 \max [-F_w, 0] + f_2 \max [-F_e, 0]) \quad (20)$$

$$A_W = (D_w + \frac{F_w}{2}) + (f_1 \max [F_e, 0] + f_1 \max [-F_w, 0] + f_2 \max [F_w, 0]) \quad (21)$$

$$A_N = (D_n - \frac{F_n}{2}) + (f_1 \max [F_n, 0] + f_1 \max [-F_s, 0] + f_2 \max [F_n, 0]) \quad (22)$$

$$A_S = (D_s + \frac{F_s}{2}) + (f_1 \max [F_n, 0] + f_1 \max [-F_s, 0] + f_2 \max [F_s, 0]) \quad (23)$$

$$A_{EE} = -f_1 \max [-F_e, 0] \quad (24)$$

$$A_{WW} = -f_1 \max [F_w, 0] \quad (25)$$

$$A_{NN} = -f_1 \max [-F_n, 0] \quad (26)$$

$$A_{SS} = -f_1 \max [F_s, 0] \quad (27)$$

$$A_P = \sum A_i \quad (28)$$

The values of f_1 and f_2 depend on the higher-order scheme to be used as shown in Table 1.

Table 1:Constants used in *A* coefficients of higher-order schemes.

Difference Scheme	f_1	f_2
Central	0	0
2nd OU	0.5	1.0
3rd OU	0.125	0.25

In equations (20)-(28), the second- and third-order upwind schemes contain two groups of terms. The first group contains the central difference terms, while the second group contains upwind-weighted corrections to these terms. The corrections are introduced to enhance the stability of the numerical scheme. Implementation of the central and hybrid schemes requires a five-point computational stencil at each node whereas the others require a nine-point stencil. To minimize algorithmic changes, all the higher-order methods are implemented via deferred correction (see Khosla and Rubin 1974). In this procedure, the coefficients are calculated initially using equations (14)-(19) for the hybrid scheme. As the solution proceeds, the higher-order scheme is slowly introduced via corrections to the source terms. At the end when the solution is fully converged, the coefficients are effectively those of the higher-order scheme outlined in equations (20)-(28).

3.2 Results for different approximations of the convection terms

The four approximations of the convection terms outlined above are applied to the two test problems over a streamwise computational domain length of 10. Computed locations of zero shear stress on the upper and lower walls are shown in Table 2 for case 1 and Table 3 for case 2. From the results of case 1, the hybrid scheme gives a large percentage difference compared to the "benchmark" result (20% for the top point and 17% for the bottom point). The artificial diffusion introduced by the hybrid coefficients makes the effective Reynolds number lower and thus the eddy lengths are shorter as would be the case in a flow with slightly lower Reynolds number. To obtain improved accuracy, a higher-order method must be used. The central and third-order upwind schemes give percentage differences under 5%, and the second-order upwind scheme under 8%.

Similar results can be seen for the points of zero shear stress for case 2. The hybrid scheme yields a maximum percentage difference (excluding the first bottom point) of around 25%. The second and third-order upwind schemes yield percentage differences (excluding the first bottom point) under 5% with the second-order upwind scheme giving the closest agreement with the "benchmark" solution. The central difference scheme yields a maximum percentage difference under 8%. It is not clear why the second-order upwind results agree best with the benchmark, in this case, which was obtained with the finite element method with bilinear elements. A possible explanation would be that both numerical schemes are roughly similar so that the comparisons contain a measure of the bias in the numerical schemes rather than providing a pure measure of accuracy.

Table 2: Points of zero shear stress, case 1

Difference Scheme	Top(% diff[a])	Bot.(% diff[a])
Hybrid	3.87(20)	5.05(17)
2nd OU	4.47(7.8)	5.70(6.6)
Central	4.64(4.3)	5.88(3.6)
3rd OU	4.61(4.9)	5.84(4.3)
Benchmark	4.85	6.10

a. Percent difference between value and benchmark solution.

Table 3: Points of zero shear stress, case 2

Difference Scheme	1st Top(%[a])	2nd Top	3rd Top	1st Bot[b]	2nd Bot	3rd Bot	4th Bot
Hybrid	1.01(17)	4.38(25)	- (-)	0.65(45)	2.14(17)	3.76(21)	6.70(25)
2nd OU	1.17(3.3)	5.50(.18)	8.20(.49)	0.36(0.0)	2.43(2.9)	4.54(.22)	8.37(.24)
Central	1.14(6.1)	5.23(5.0)	7.65(6.7)	0.44(18)	2.41(3.7)	4.32(5.3)	7.99(4.9)
3rd OU	1.16(4.3)	5.32(3.2)	7.78(4.9)	0.43(16)	2.43(2.9)	4.39(3.6)	8.10(3.6)
Benchmark	1.21	5.49	8.16	0.36	2.50	4.55	8.39

a. Percent difference between value and benchmark solution.
b. This corner eddy is too small to be determined accurately on the scales of interest here.

The order of the difference schemes can be estimated following generalizations of the Richardson extrapolation method to be described in detail in the next section. Basically, the exact functional value can be approximated in terms of results on finite grids plus the leading term of the truncation error as:

$$\phi = \phi_h + h^n x_n + \ldots \tag{29}$$

$$\phi = \phi_{2h} + (2h)^n x_n + \ldots \tag{30}$$

$$\phi = \phi_{4h} + (4h)^n x_n + \ldots \tag{31}$$

where h is the grid spacing in the x-direction, n is the order of the scheme and x_n is a grid function, which is assumed to be equal for the h, $2h$, and $4h$ grids. The grid function contains spatial derivatives of ϕ with respect to x and y, which are also of order n. The statements above will be valid so long as h is sufficiently small for the leading term to be dominant. The order of the numerical scheme can then be estimated from:

$$n = \frac{ln\left[\frac{(\phi_{2h} - \phi_{4h})}{(\phi_h - \phi_{2h})}\right]}{ln(2)} \tag{32}$$

Computations were made on the standard grid (258 x 34) and two sets of coarser grids (130 x 18 and 66 x 10) for the isothermal backward facing step (equivalent to case 1) but at a Reynolds number of 100. The lower Reynolds number was chosen for economy because the value of h required for equations (29)-(32) to be valid is larger at lower Reynolds numbers. For example, the analysis was applied to computations on these 3 sets of grids for case 1 at a Reynolds number of 400 using the hybrid scheme. Equation (32) estimated the hybrid scheme to be of *0th* order, which is clearly incorrect. Obviously, at this Reynolds number the coarser grids are not sufficiently fine for the leading term in the truncation series to be dominant. For the lower Reynolds number, estimates of the order of the numerical scheme based on equation (32) are presented in Table 4. The results show that the 1st OU scheme is indeed first-order accurate, the 2nd OU and central schemes are second-order accurate, and the 3rd OU is only slightly better than the second-order

accurate. The only possible surprise is that the hybrid scheme is almost second-order accurate. This is mainly due to the lower Reynolds number of the flow which enables the use of central differencing in major sections of the computational domain. The ability of the scheme to adapt to flow conditions to improve its order of accuracy is one of the reasons for its popularity, but the uncertainty concerning its order of accuracy in different flow situations makes it unreliable for use in a general purpose computer code.

Table 4: Estimated order of numerical schemes, case 1 @ Re = 100

Difference Scheme	1st OU	Hybrid	2nd OU	Central	3rd OU
Order	0.8	1.9	2.0	2.0	2.2

4 DISCRETIZATION ERROR

4.1 Richardson Extrapolation

The discretization error was investigated by employing a Richardson extrapolation method of analysis. Grid 3 described in section 2 with a domain length of 10 units was used as a base grid. This grid will be defined as the $2h$ grid. A grid was generated with half the grid spacing in the x and y directions which is defined as the h grid, and one was generated with double the grid spacing, defined as the $4h$ grid. The sizes of these grids are displayed in Table 5.

Table 5: Grids used in Richardson extrapolation

Grid	Grid size
h	743x81
$2h$	372x41
$4h$	187x21

Central differencing was used for the convection terms of the governing equations. This scheme, described in detail in the previous section, is second-order accurate. The error for the three grids can be written as a Taylor series following Ferziger (1989):

$$\varepsilon_h = h^2 x_2 + h^4 x_4 + \ldots \tag{33}$$

$$\varepsilon_{2h} = 4h^2 x_2 + 16h^4 x_4 + \ldots \tag{34}$$

$$\varepsilon_{4h} = 16h^2 x_2 + 256h^4 x_4 + \ldots \tag{35}$$

If h is sufficiently small so that the first term on the right hand side of equations (33)-(35) dominates, any property ϕ can be written as:

$$\phi = \phi_h + \varepsilon_h \tag{36}$$

$$\phi = \phi_{2h} + \varepsilon_{2h} \tag{37}$$

$$\phi = \phi_{4h} + \varepsilon_{4h} \tag{38}$$

Equations (33)-(35) are substituted into equations (36)-(38) respectively, to give:

$$\phi = \phi_h + h^2 x_2 \tag{39}$$

$$\phi = \phi_{2h} + 4h^2 x_2 \tag{40}$$

$$\phi = \phi_{4h} + 16h^2 x_3 \tag{41}$$

Equation (39) is set equal to (40):

$$\phi_h - \phi_{2h} = 3h^2 x_2 \tag{42}$$

From equation (33):

$$\varepsilon_h = h^2 x_2 \tag{43}$$

Equation (43) can be used in equation (42) to obtain an expression for the error on the h grid:

$$\varepsilon_h = \frac{\phi_h - \phi_{2h}}{3} \tag{44}$$

The error estimate given by equation (44) is used to eliminate the $h^2 x_2$ truncation error term in equation (33) and give a result which is fourth-order accurate as:

$$\phi_{2h}\big|_{4th} = \frac{4}{3}\phi_h\big|_{2nd} - \frac{1}{3}\phi_{2h}\big|_{2nd} \tag{45}$$

Note that this result is generated on the $2h$ grid, since equation (45) requires a fine grid (h) and a standard grid ($2h$) value at each location the equation is applied.

Similarly, one can combine results on the $2h$ and $4h$ grids to yield:

$$\phi_{4h}\big|_{4th} = \frac{4}{3}\phi_{2h}\big|_{2nd} - \frac{1}{3}\phi_{4h}\big|_{2nd} \tag{46}$$

Equation (46) gives fourth-order accurate results from the $2h$ and $4h$ grid values. Sixth-order accurate results can be obtained by eliminating the second term in equations (33)-(35) which assumes:

$$\varepsilon_{2h}\big|_{4th} = 16h^4 x_4 \tag{47}$$

$$\varepsilon_{4h}\big|_{4th} = 256h^4 x_4 \tag{48}$$

The sixth-order accurate result takes the form:

$$\phi_{4h}\big|_{6th} = \phi_{2h}\big|_{4th} + 16h^4 x_4 \tag{49}$$

$$\phi_{4h}\big|_{6th} = \phi_{4h}\big|_{4th} + 256h^4 x_4 \tag{50}$$

By equating equations (49) and (50) and following the procedure outlined above, the fourth-order accurate truncation error is estimated as:

$$\varepsilon_h = \frac{\phi_{2h} - \phi_{4h}}{15} \tag{51}$$

The fourth-order accurate result can be corrected to obtain a sixth-order accurate result as:

$$\phi_{4h}\big|_{6th} = \frac{16}{15}\phi_{2h}\big|_{4th} - \frac{1}{15}\phi_{4h}\big|_{4th} \tag{52}$$

Again this result is obtained on the *4h* grid. The procedure used to generate the more accurate results in equations (45) and (52) are equivalent to those for estimating zero-grid-size results (see Churchill et al., 1981). The present results may also be interpreted as the *0h* results for the second-order scheme.

4.2 Application to case 1

As an example of the estimation of discretization error, the points of zero shear stress at the upper and lower walls are calculated. The results of these calculations as well as the extrapolated values using equations (45), (46), and (52) are displayed in Table 6, and compared to the "benchmark" solution.

Table 6: Points of zero shear stress, case 1

Grid	Top(% diff[a])	Bot.(% diff[a])
$h\|_{2nd}$ [b]	4.72(-2.6)	6.01(-1.5)
$2h\|_{2nd}$	4.55(-6.1)	5.79(-5.1)
$4h\|_{2nd}$	3.61(-25)	4.76(-22)
$2h\|_{4th}$	4.78(-1.4)	6.08(-0.26)
$4h\|_{4th}$	4.87(0.41)	6.13(0.52)
$4h\|_{6th}$	4.77(-1.6)	6.08(-0.31)
Benchmark	4.85	6.10

a. Percent difference between value and benchmark solution.
b. Results incompletely converged to $r_{max} = 1.5\text{x}10^{-2}$(maximum of u, v, and mass equation residual), all other results converged to $r_{max} = 2.0\text{x}10^{-4}$.

The results using Richardson extrapolation show that combining the $2h|_{2nd}$and $4h|_{2nd}$ results, yields an improved result. For the top wall point, the percentage difference improves from 6.1% (*2h* grid) and 25%(*4h* grid) to 0.41%(*4h* grid, fourth-order accurate). The bottom wall point percentage difference improves from 5.1% (*2h* grid) and 22%(*4h* grid) to 0.26%(*4h* grid, fourth-order accurate). The initial results on the *h* grid are not converged to the same level as the *2h* and *4h* grid results. This may partly explain why the $2h|_{4th}$ results are not much better than the $4h|_{4th}$ results.

4.3 Application to case2

Similar analysis is applied to test case 2 with calculations completed on the *2h* and *4h* grid only. The *h* grid results did not converge fully after 16,000 iterations so they are not included in the analysis. The trends are similar to those for case 1. The results are shown in Table 7.

Table 7: Points of zero shear stress, case 2

Grid[a]	1st Top(%[b])	2nd Top	3rd Top	1st Bot[c]	2nd Bot	3rd Bot	4th Bot
$2h\|_{2nd}$	1.19(1.7)	5.30(3.5)	7.75(5.0)	0.47(31)	2.46(1.6)	4.39(3.5)	8.10(3.5)
$4h\|_{2nd}$	1.02(16)	4.75(16)	6.93(18)	0.62(42)	2.21(13)	3.92(16)	7.45(11)
$4h\|_{4th}$	1.25(3.2)	5.48(.18)	8.02(1.8)	0.42(14)	2.54(1.6)	4.55(0.0)	8.32(.84)
Benchmark	1.21	5.49	8.16	0.36	2.50	4.55	8.39

a. All results converged to $r_{max} = 5.0\text{x}10^{-3}$.
b. Percent difference between value and benchmark solution.
c. This corner eddy is too small to be determined accurately on the scales of interest here.

5 OUTFLOW BOUNDARY CONDITIONS

5.1 Description of boundary conditions

Most of the boundary conditions are straightforward to specify as discussed in section 2, except for the location of the outflow plane. The usual practice is to locate this plane far enough away from the region of interest which presumes a pre-knowledge of the solution. The question arises as to how far the outflow plane should be located in separated flows and what errors are introduced by too short a location. The effect of the location of the outflow boundary has been investigated for the two test cases.

The outflow boundary condition (OBC) for test case 1 consists of setting the first derivatives of u and v, in the direction normal to the outflow plane, to zero, while satisfying global conservation of mass at the outflow. Thus:

$$\Delta u = \int_{-0.5}^{0.5} (u_{2,j} - u_{n-1,j})\, dy \tag{53}$$

$$\frac{\partial u}{\partial x} \approx 0 \Rightarrow u_{n,j} = u_{n-1,j} + \Delta u \tag{54}$$

$$\frac{\partial v}{\partial x} = 0 \Rightarrow v_{n,j} = v_{n-1,j} \tag{55}$$

where the subscripts 2 and n denote the inflow and outflow locations respectively for the u variable. If global continuity is satisfied at the outflow $\Delta u = 0$ and $u_{n,j} = u_{n-1,j}$.

The OBC for test case 2 is similar to that of test case 1, with the additional boundary condition for the temperature equation being:

$$\frac{\partial T}{\partial x} = 0 \Rightarrow T_{n,j} = T_{n-1,j} \tag{56}$$

The OBCs for the two model problems are tested by obtaining solutions on four streamwise domain lengths. As discussed in section 2, the four domain lengths are 30, 15, 10, and 7.

5.2 Results - Case 1

The points of zero wall shear stress are calculated and shown in Table 8, while the streamlines and pressure contours are shown in Figures 5 and 6 for the various domain lengths. It is clear that with the outflow boundary conditions specified in equations (53) to (56) the location of the outflow boundary has little effect on the computed solution. There was no difficulty in obtaining the correct results even though a recirculating eddy was dissected by this boundary for the domain of 7.

Table 8: Points of zero wall shear stress, case 1

Domain Length	30	15	10	7	% diff[a]
1st Top	4.57	4.56	4.55	4.53	-0.66
2nd Top	10.27	10.27	-	-	-
1st Bot.	5.80	5.80	5.78	5.76	-0.69

a. Percent difference between long (L=15) and short (L=7) domain.

5.3 Results - Case 2

The points of zero wall shear stress for case 2 are shown in Table 9, while the streamlines, pressure, and temperature contours are shown in Figures 7 - 9. The observation above of little influence of the location of outflow boundary, is also true. As shown by Wilson et al. (1991), other boundary conditions such as zero second derivatives normal to the outflow plane are not as successful. Only the present boundary conditions (equations 53-56) enabled the pressure variation across the outflow plane in Figures 6 and 8 to be correctly predicted for the shortest domain length of 7.

Table 9: Points of zero wall shear stress, case2

Domain Length	30	15	10	7	% diff[a]
1st Top	1.18	1.18	1.19	1.20	1.7
2nd Top	5.29	5.29	5.30	5.24	-0.95
3rd Top	7.91	7.91	7.75	-	-
4th Top	10.19	10.19	-	-	-
1st Bot.	0.47	0.47	0.47	0.47	0.0
2nd Bot.	2.45	2.45	2.46	2.47	0.82
3rd Bot.	4.38	4.38	4.39	4.35	-0.68
4th Bot.	8.25	8.25	8.10	-	-

a. Percent difference between long (L=15) and short (L=7) domain.

6 INCOMPLETE ITERATIVE CONVERGENCE

6.1 Stopping criteria and error estimation

Uncertainty due to incomplete iterative convergence can be defined as the difference between the current and the exact solution of the discretized problem on the same grid. The discretized solution will never satisfy the continuous equations exactly. Therefore, there will be a point in the iteration process when further relaxation of the system of equations will not bring any additional improvement in the solution. Stopping criteria must be selected, and the resulting errors from foregoing additional iterations, must be estimated. One stopping criterion, which is common in practice, is to terminate the iterative process when the difference in computed results, from one iteration to the next, falls below a pre-selected amount. Another stopping criterion is based on a measure of how well the discretized solution satisfies the discretized equations. This quantity is referred to as the residual of the discretized equation. In this method, when the residual falls below a pre-selected amount, the iterations are stopped.

A method has been proposed by Ferziger (1989) that is based on not only the difference of successive iterates but also on the rate of convergence. The uncertainty due to incomplete iterative convergence can also be estimated. The solution after the n^{th} iteration can be written as:

$$\phi^n = \tilde{\phi} + \varepsilon^n \tag{57}$$

where ϕ^n is the solution after n iterations, $\tilde{\phi}$ is the desired converged solution, and ε^n is the error due to incomplete convergence. The iterative scheme for a linear system can be simplified as:

$$\phi^{n+1} = A\phi^n + S \tag{58}$$

where A is the amplification matrix that transforms the solution after n iterations, ϕ^n, to ϕ^{n+1} after adding an effective source term, S. If equations (57) and (58) are combined, it can be shown that the error obeys the homogeneous form of equation (58). The eigenvalues and eigenfunctions are calculated from:

$$A\psi_k = \lambda_k \psi_k \tag{59}$$

The initial error ε^0 can be written as a generalized Fourier series:

$$\varepsilon^0 = \sum_{k=1}^{n} a_k \psi_k \tag{60}$$

Equation (60) can be used in (57) to develop an expression for the solution after n iterations as:

$$\phi^n = \tilde{\phi} + \sum_{k=1}^{n} a_k \lambda_k^n \psi_k \tag{61}$$

If it is assumed that λ_1 will dominate after many iterations, equation (61) can be replaced with a simplified expression:

$$\phi^n = \tilde{\phi} + a_1 \lambda_1^n \psi_1 \tag{62}$$

Equation (62) can be written using the indices $n-1$, n, and $n+1$ to yield an estimate for the principal eigenvalue:

$$\lambda_1 \approx \frac{\phi^{n+1} - \phi^n}{\phi^n - \phi^{n-1}} \tag{63}$$

An estimate of the principal eigenvalue, applicable to all nodes, can be obtained as the ratio of the *L2*-norms of the numerator and denominator of equation (63). If equation (62) is rearranged, an estimate of the convergence error can be calculated as:

$$\varepsilon^n \approx \frac{\phi^{n+1} - \phi^n}{\lambda_1 - 1} \tag{64}$$

The result of equation (64) is that the convergence error depends on the difference in the solution from iteration to iteration *plus* the rate of convergence. This means that a given difference between successive iterates will yield different convergence errors depending on the principal eigenvalue for the iteration matrix. Therefore, if the iterative method exhibits poor convergence, the principle eigenvalue of the iteration matrix A will be close to unity. This will make it difficult to reduce the convergence error ε^n because the inverse of the denominator of equation (64) will be large. This result can form the basis for stopping criteria. When the convergence error, defined by equation (64), falls below a predetermined level, the iterations can be terminated.

6.2 Application to model problems

The convergence error was estimated for cases 1 and 2 by using the u component of velocity for the general variable ϕ in equations (57)-(64). The convergence error is shown in Figure 10. In addition, the norm of the residuals of the u momentum, v momentum, and continuity equations is shown in Figure 11. The evolutions of the recirculation zones, determined by the points of zero shear stress at the upper and lower walls, are also monitored throughout the iterative process. They are shown in Figure 12 and 13 for cases 1 and 2, respectively. This gives an indication when additional computational work will not change the solution.

In Figure 12, the first point of zero wall shear stress for case 1 on the top wall and the length of the bottom recirculation zone remain constant after approximately 3000 iterations. This implies that the shear stress along the top wall is relatively constant and that the solution is not changing. From Figure 11, the norm of the u, v, and mass equation residuals at this point is 2×10^{-3} and the estimated convergence error is about 1×10^{-3}. It appears that this is an appropriate stopping point.

As shown in Figure 13, the three recirculation zone lengths for case 2 remain constant after approximately 3200 iterations. Note that the second bottom eddy is the last to attain a constant length. Figure 11 shows that the norm of the residuals at this point is approximately 6×10^{-3}, and the estimated convergence error is approximately 6×10^{-3}.

Figures 10 and 11 have similar trends and values. For case 1, the norm of the residuals (Figure 11)

follows roughly the same constant slope throughout the iterative process. The mean value of the convergence error, (Figure 10) also follows the same slope shown in Figure 11. The values of the norm and convergence error are also similar. For case 2, the residual norm follows the same slope as case 1 until about 800 iterations, after which it decreases at a slower rate. The mean value of the convergence error also shows the same behavior. The residuals shown in Figure 11 have been plotted using the *L2*-norm of the *u* momentum, *v* momentum, and continuity equations, while Figure 10 uses the error estimate of the *u* component of velocity.

For the two test cases, both the norm of the residuals and the estimate of the convergence error appear to be appropriate stopping criteria.

7 COMPUTATIONAL GRID ASPECT RATIO

7.1 Choice of grid-cell aspect ratio

In most computational fluid flow problems, the choice of the grid-cell aspect ratio is not trivial. Convergence characteristics suggest that the aspect ratio should be of order unity, but the need to resolve boundary layers may dictate much higher aspect ratios. The natural way to carry out grid refinement is to halve the cell size in each direction, which automatically maintains the initial cell aspect ratio. What is the effect of this choice on the accuracy of computed results?

Assuming that the leading truncation error term is of second-order and that the grid spacing is sufficiently small, the functional value, ϕ, can be written as:

$$\phi = \phi_h + \frac{h_x^2}{2}\frac{\partial^2\phi}{\partial x^2} + \frac{h_y^2}{2}\frac{\partial^2\phi}{\partial y^2} + \ldots \tag{65}$$

where h_x and h_y are the grid spacing in the x and y directions, respectively.

Let the aspect ratio be defined as, $A_R = h_x/h_y$, also let $\beta = \frac{\partial^2\phi}{\partial y^2} \Big/ \frac{\partial^2\phi}{\partial x^2}$ then:

$$\phi = \phi_h + \frac{h_x^2}{2}\frac{\partial^2\phi}{\partial x^2}\left(1 + \frac{\beta}{A_R^2}\right) + \ldots \tag{66}$$

The discretization error is then approximately:

$$\varepsilon = \frac{h_x^2}{2}\frac{\partial^2\phi}{\partial x^2}\left(1 + \frac{\beta}{A_R^2}\right) \tag{67}$$

For the same total number of grid points, refinement may be selectively in the x or y-direction. The choice would produce a change in the cell-aspect ratio. For example, if h_y is reduced by a factor m, with h_x (=h) unchanged, A_R will be increased by the factor m. Then the discretization error would be approximately:

$$\varepsilon_1 = \frac{h^2}{2}\frac{\partial^2\phi}{\partial x^2}\left(1 + \frac{\beta}{m^2 A_R^2}\right) \tag{68}$$

On the other hand, if h_y is unchanged while h_x is reduced by a factor m so that $h_x = h/m$ and A_R is also reduced by a factor m, the error is:

$$\varepsilon_2 = \frac{h^2}{2}\frac{\partial^2\phi}{\partial x^2}\left(\frac{1}{m^2} + \frac{\beta}{A_R^2}\right) \tag{69}$$

The ratio of the errors is then:

$$\frac{\varepsilon_1}{\varepsilon_2} = \frac{1 + \dfrac{\beta}{m^2 A_R^2}}{\dfrac{1}{m^2} + \dfrac{\beta}{A_R^2}} = \frac{\dfrac{A_R^2}{\beta} + \dfrac{1}{m^2}}{\dfrac{A_R^2}{m^2\beta} + 1} \tag{70}$$

The implication of this result is that:

$$\frac{\varepsilon_1}{\varepsilon_2} = 1, \text{if } A_R{}^2 = \beta \tag{71}$$

$$\frac{\varepsilon_1}{\varepsilon_2} < 1, \text{ if } A_R{}^2 < \beta$$

$$\frac{\varepsilon_1}{\varepsilon_2} > 1, \text{ if } A_R{}^2 > \beta$$

Therefore the limiting cell aspect ratio for selective grid refinement is $\sqrt{\beta}$, or $\sqrt{\frac{\partial^2\phi}{\partial y^2}/\frac{\partial^2\phi}{\partial x^2}}$. So long as $A_R < \sqrt{\beta}$ grid refinement in the y-direction leads to more effective error reduction than in the x-direction. If $A_R > \sqrt{\beta}$ further grid refinement in the y-direction becomes less effective than that in the x-direction. In boundary-layer type flows $\beta >> 1$, so the optimum value of $A_R > 1$. But in separated flows with no preferred direction $\beta \sim 1$ and the optimum A_R will also be about 1.

7.2 Application to model problems

To explore these effects, computations of case 1 were made on several grids with cell aspect ratios in the range of 0.625 to 5.0. Both hybrid and central difference schemes were utilized because it was difficult to get converged solutions with the latter on coarser grids because of wiggles generated by the well-known "odd-even" decoupling problem. The results for the hybrid scheme are presented in Table 10 and those for the central scheme in Table 11. Grids 1-3 have the same cell-size in the x-direction, but the y-direction cell-sizes were halved in 2 and halved again in 3. Grids 4 and 5 have the same y-direction cell-sizes as grids 2 and 3, respectively, but doubled x-direction cell-sizes. Correspondingly, the aspect ratios are doubled. The results show improved agreement with the benchmark solution with refinement in the y-direction corresponding to increased aspect ratio. For example, in Table 10 grids 2 and 5 have the same total number of points but the case with the higher aspect ratio gives better agreement with the benchmark. This confirms the analysis for large β. The same applies to grids 1 and 4. Results in Table 11 for the central difference scheme show that the deviation from the benchmark was reduced by a factor of 4 simply by halving the cell-size in the y-direction. For the second-order scheme, such a reduction would normally

be expected from halving of the cell size in both directions. Clearly, the y-component of the truncation error is dominant and selective refinement in this direction is more cost effective than a global refinement. This cannot be presented as a panacea for all two-dimensional separated flows, but will depend on the characteristics of the flow and the extent of deviation from an elongated boundary-layer character. The closer large regions of the flow are to boundary-layer type flows, and hence, the larger β is, the more will be the tendency for large cell aspect ratios to produce more accurate solutions. For separated flows with little or no elongated regions with boundary-layer type flows, aspect ratios of order unity would be the most effective.

Table 10: Points of zero wall shear stress, hybrid difference scheme, case 1.

Grid	Grid Size	Aspect Ratio	1st Top(%[a])	1st Bot
1	258 x 18	0.625	2.36(51.3)	3.52(42.3)
2	258 x 34	1.25	3.87(20.2)	5.04(17.4)
3	258 x 66	2.5	4.53(6.6)	5.76(5.6)
4	130 x 34	2.5	3.33(31.3)	4.42(27.6)
5	130 x 66	5	4.12(15.1)	5.30(13.1)
Benchmark	-	-	4.85	6.10

a. Percent difference between value and benchmark solution

Table 11: Points of zero wall shear stress, central difference scheme, case 1.

Grid	Grid Size	Aspect Ratio	1st Top(%[a])	1st Bot
1	258 x 18	0.625	--[b]	--[b]
2	258 x 34	1.25	4.64(4.3)	5.88(3.6)
3	258 x 66	2.5	4.80(1.0)	6.05(0.8)
Benchmark	-	-	4.85	6.10

a. Percent difference between value and benchmark solution
b. Solution not converged.

8 CONCLUDING REMARKS

Various sources of uncertainty in numerical computations of fluid flow have been examined. Specific estimates of numerical error magnitudes were computed with reference to two two-dimensional separated flow problems. Truncation error in numerical schemes can be estimated by comparing solutions from low and higher-order schemes. The effect of outflow boundary conditions can be estimated by varying systematically the location of the outflow boundary without changing the grid distribution or the numerical scheme. Discretization errors can be estimated by

making computations on related grids with varying degrees of fineness and using Richardson extrapolation method. The solution can then be improved. The method can also be used to determine the global order of accuracy of a numerical method. The uncertainty in computed results due to incomplete convergence of the iterative scheme can be removed by computing an estimate of the convergence error and using this as a stopping criterion rather than the more widely used change in computed results between iterates. Grid aspect ratio effects on the solution are also important. Higher aspect ratios are more effective in generating accurate solutions in separated flows with elongated regions with boundary layer character.

ACKNOWLEDGMENT

Computations were performed on the Cray computers at NASA Langley Research Center, Hampton, Virginia.

REFERENCES

Churchill, S.W., Chao, P., and Ozoe, H., 1981 "Extrapolation of Finite-Difference Calculations of Laminar Natural Convection In Enclosures to Zero Grid Size," Numer. Heat Transfer, Vol 4, pp 39-51.

Dang, A.L., Kehtarnavaz, H., and Coats, D.E., 1989 "The Use of Richardson Extrapolation in PNS Solutions of Rocket Nozzle Flow" AIAA Paper 89-2895.

de Vahl Davis, G., 1983 "Natural Convection of Air In a Square Cavity: A Bench Mark Numerical Solution," Int. J. Numer. Methods Fluids, Vol 3, pp. 249-264.

Ferziger, J.H., 1989 "Estimation and Reduction of Numerical Error, Forum on Methods of Estimating Uncertainty Limits in Fluid Flow Computations," ASME Winter Annual Meeting, San Francisco.

Gartling, D.K., 1990 "A Test Problem for Outflow Boundary Conditions - Flow Over a Backward Facing Step," Int. J. Numer. Methods Fluids, Vol 11, pp. 953-967.

Khosla, P.K., and Rubin, S.G., 1974 "A Diagonally Dominant Second-Order Accurate Implicit Scheme," Computers and Fluids, Vol 2, pp.207-209.

Leone J.M. Jr., 1990 "Open Boundary Condition Symposium Benchmark Solution: Stratified Flow Over a Backward-Facing Step," Int. J. Numer. Methods Fluids, Vol 11, pp. 969-984.

Richardson, L.F., 1911 "The Approximate Arithmetical Solution by Finite Differences of Physical Problems," Philos. Trans. R. Soc. London Ser. A, Vol 210, pp. 307-357.

Richardson, L.F., and Gaunt, J.A., 1927 "The Deferred Approach to the Limit," Philos. Trans. R. Soc. London Ser. A, Vol 226, pp. 299-361.

Patankar, S.V., and Spalding, D.B., 1972 "A Novel Finite Difference Formulation for Differential Expressions Involving both First and Second Derivatives, Int. J. Numer. Methods Eng., Vol 4, pp. 551-559.

Wilson, R.V., Demuren, A.O., and Hagstrom, T. 1991 "Test Case 1: Flow Over a Backward-Facing Step," Minisymposium on Outflow Boundary Conditions, Stanford University.

Wilson, R.V., Demuren, A.O., and Hagstrom, T. 1991 "Test Case 2: Stratified Flow Over a Backward-Facing Step," Minisymposium on Outflow Boundary Conditions, Stanford University.

Zing, D.W., 1991 "Viscous Airfoil Computations Using Richardson Extrapolation", AIAA Paper 91-1559.

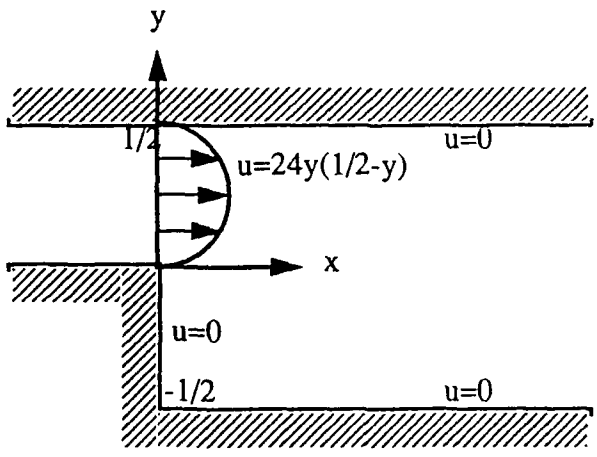

Figure 1. Geometry for case 1, Isothermal backward facing step.

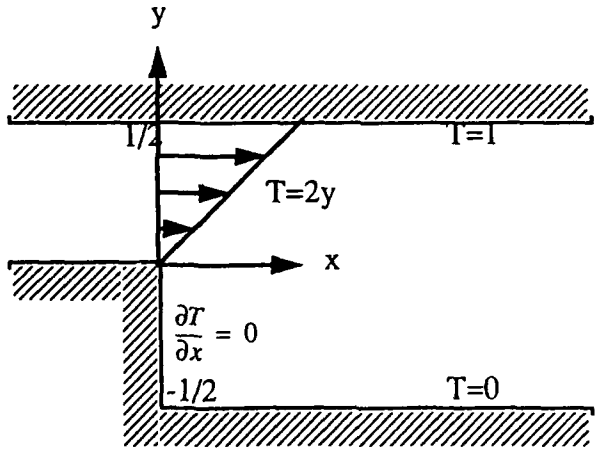

Figure 2. Geometry for case 2, Stratified backward facing step. Same velocity boundary conditions as case 1.

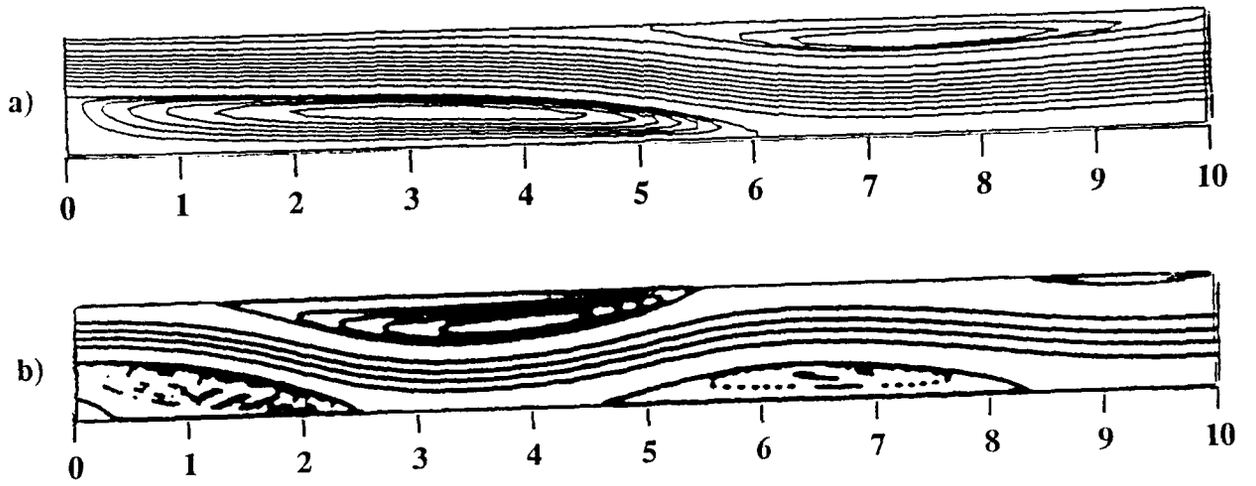

Figure 3. "Benchmark" streamfunction contours
a) Case 1, Gartling (1990), b) Case 2, Leone (1990).

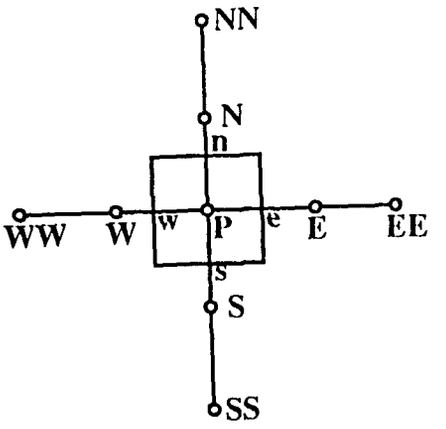

Figure 4. Typical control volume

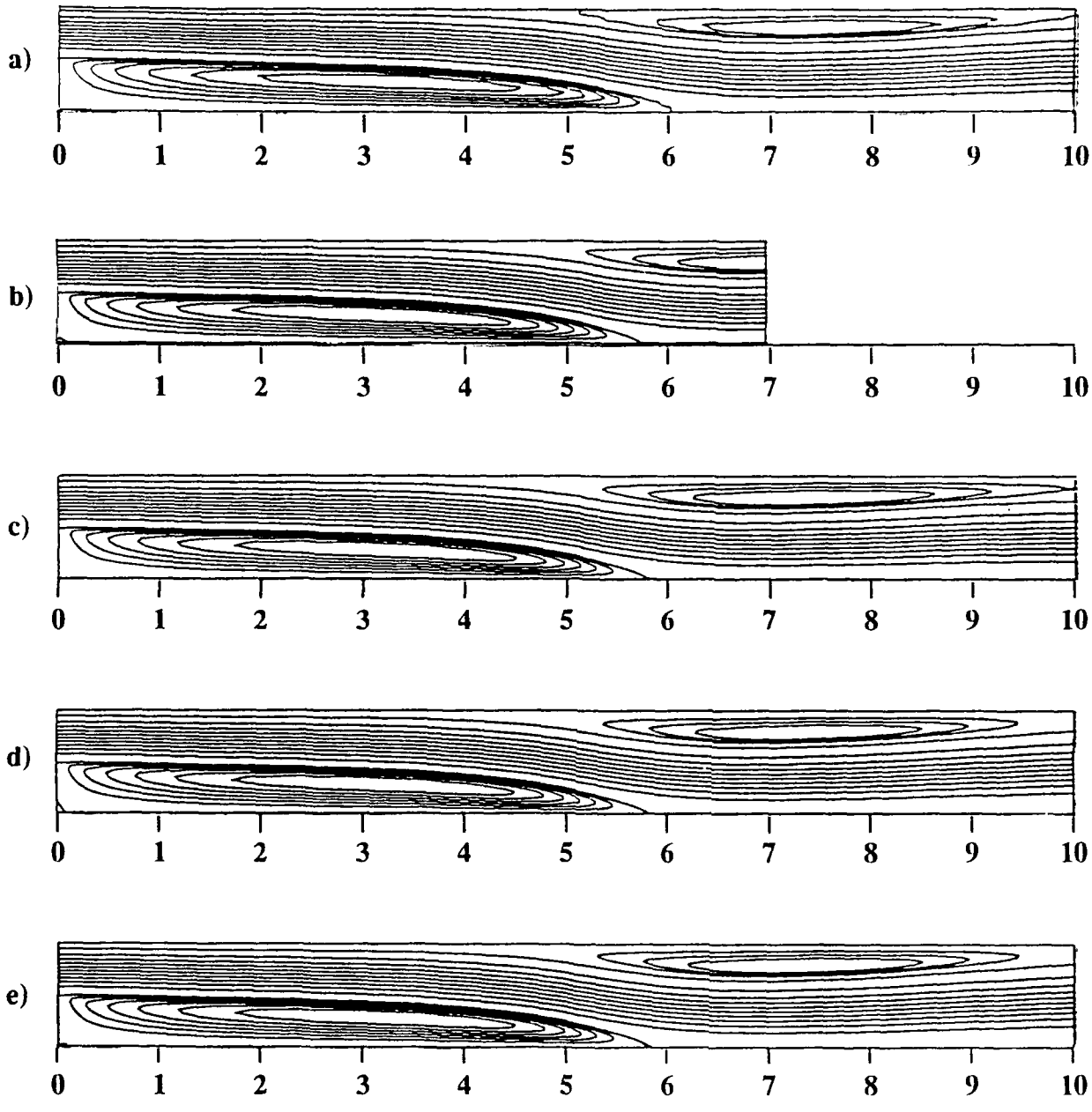

Figure 5. Normalized streamlines, case 1
a) "Benchmark" solution, b) L=7, c) L=10, d) L=15, e) L=30

Level values are: -0.030, -0.025, -0.020, -0.015, -0.010. -0.005, 0.0, 0.050, 0.100, 0.150, 0.200, 0.250, 0.300, 0.350, 0.400, 0.450, 0.490, 0.500, 0.502, 0.504.

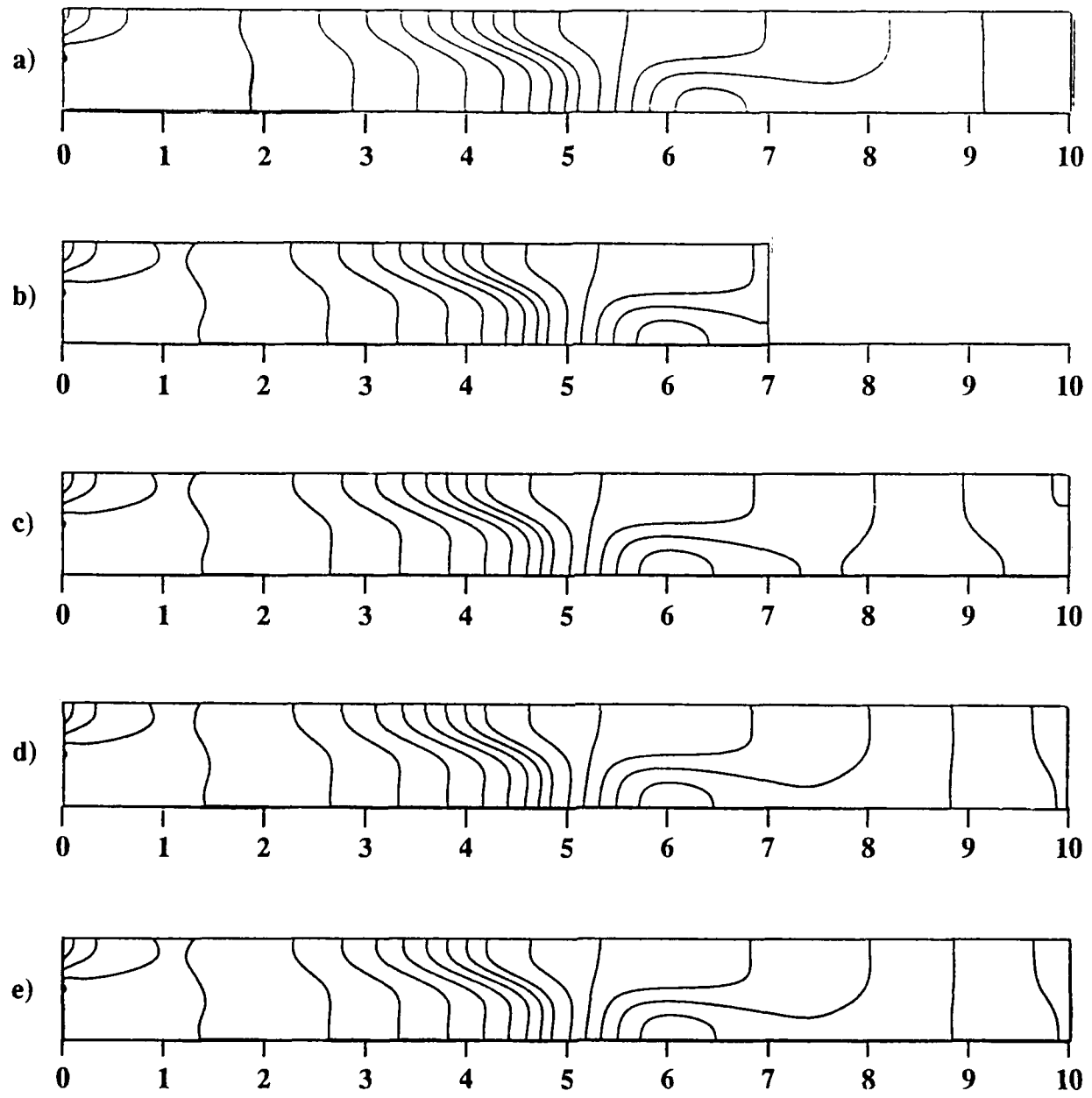

Figure 6. Normalized pressure contours, case 1
a) "Benchmark" solution, b) L=7, c) L=10, d) L=15, e) L=30

Level values are: 0.01, 0.02, 0.03, 0.04, 0.05, 0.06, 0.07, 0.08, 0.09, 0.10, 0.12, 0.14, 0.16, 0.018, 0.20, 0.22, 0.24.

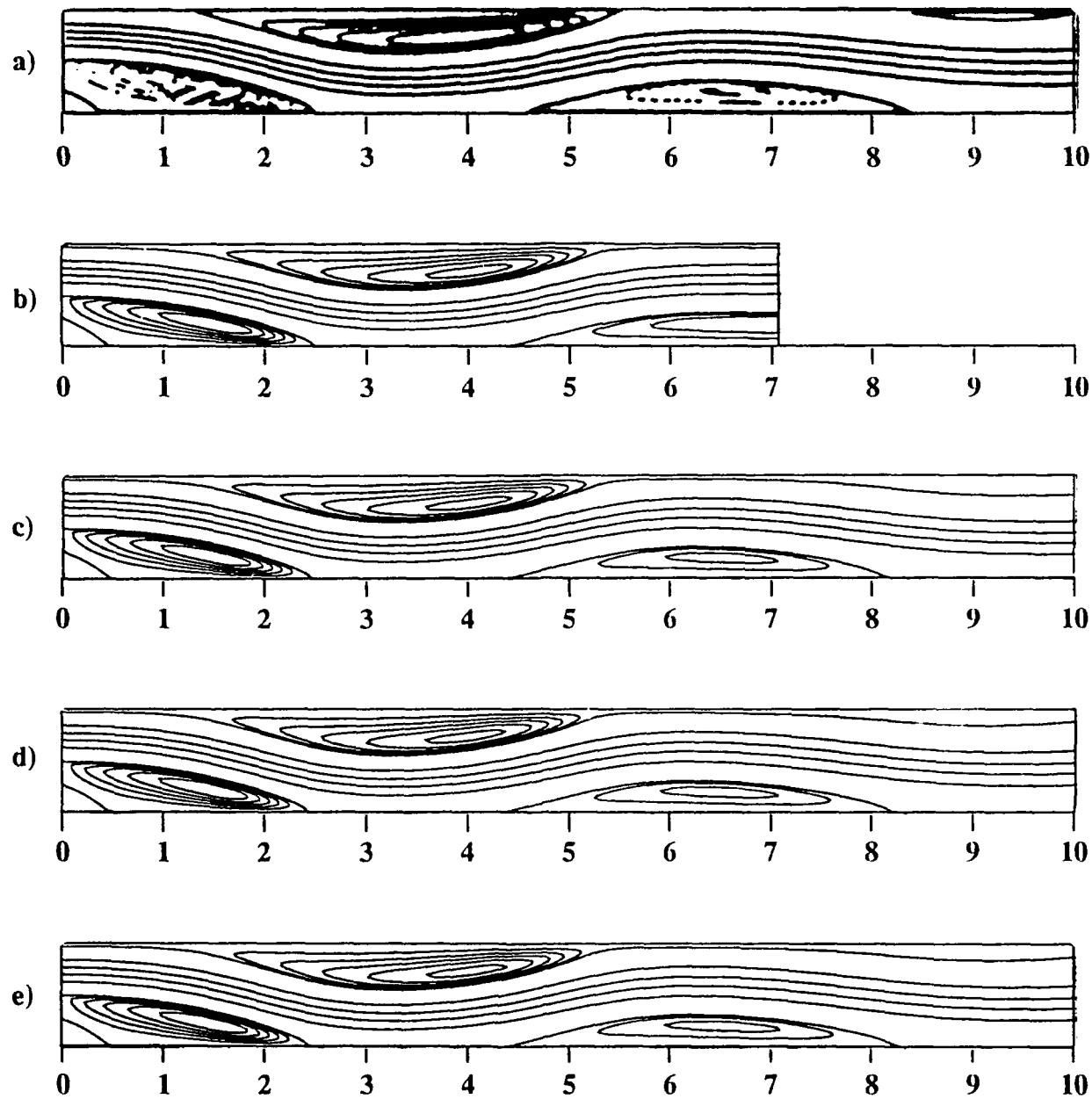

Figure 7. Normalized streamlines, case 2
a) "Benchmark" solution, b) L=7, c) L=10, d) L=15, e) L=30

Level values are: 0.0994 in the main flow (between the separated streamlines) and 0.004 within the eddies.

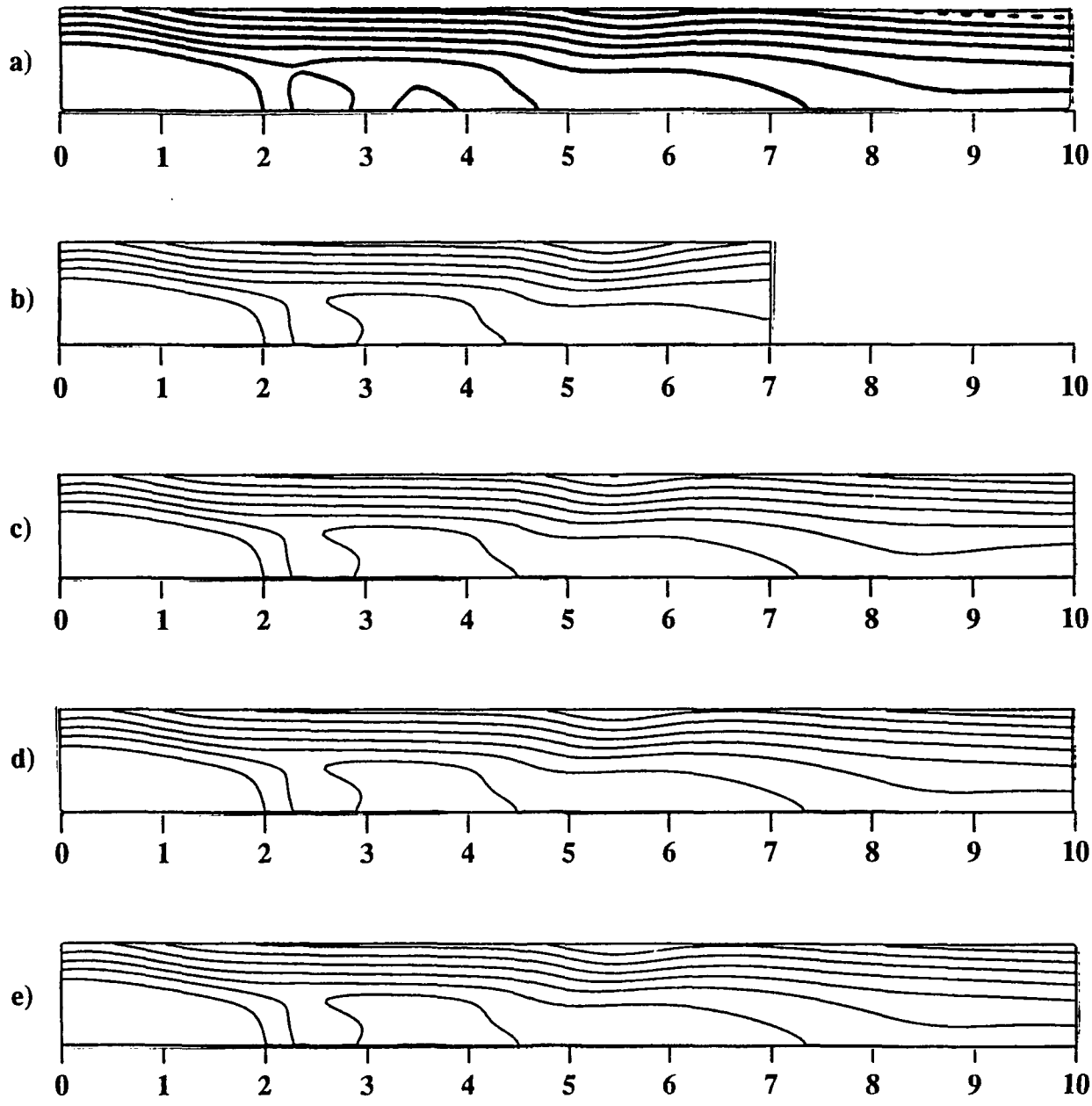

Figure 8. Normalized pressure contours, case 2
a) "Benchmark" solution, b) L=7, c) L=10, d) L=15, e) L=30

Level values are: 0.00 at step corner, 0.04841 increments.

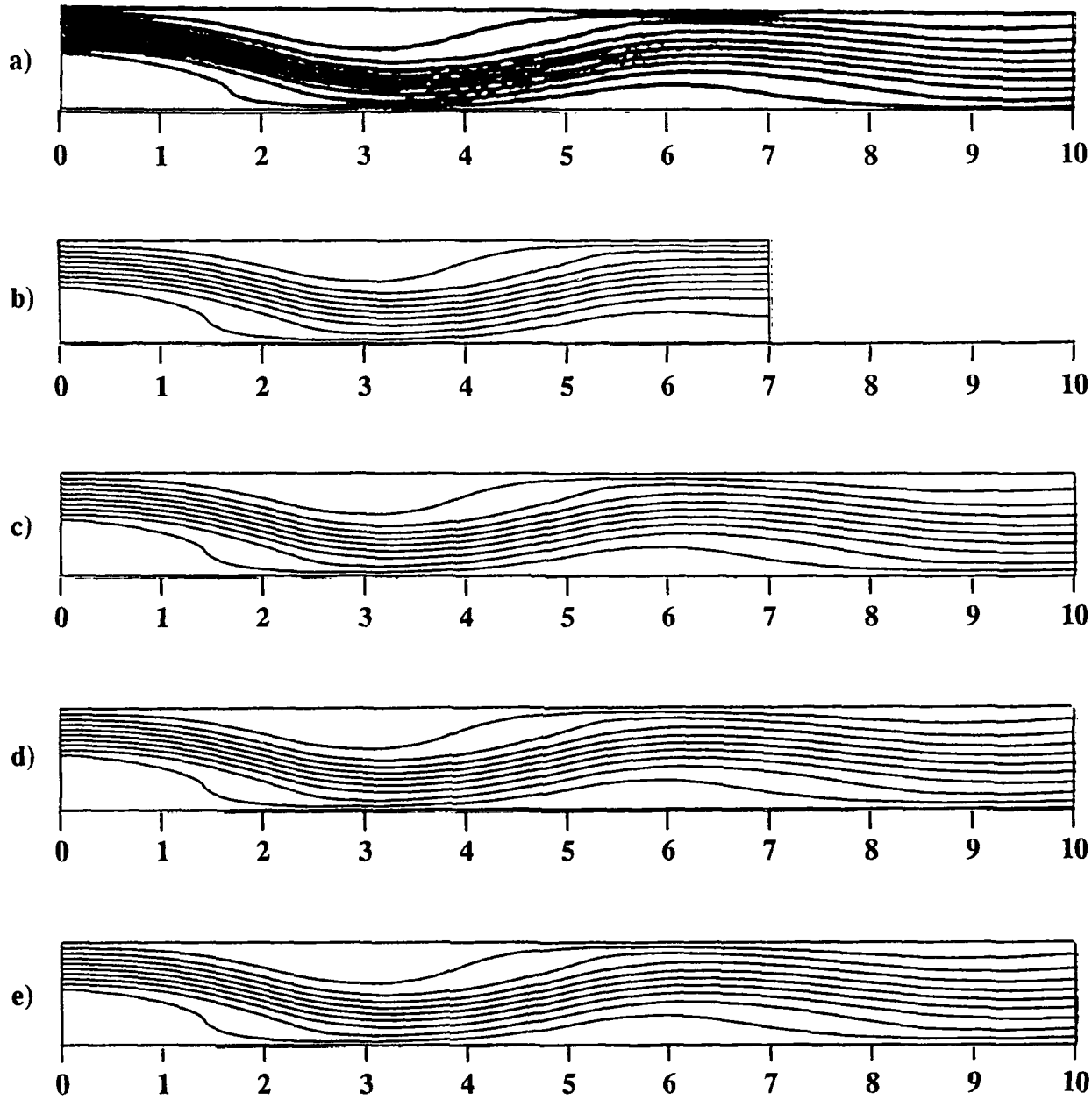

Figure 9. Normalized temperature contours, case 2
a) "Benchmark" solution, b) L=7, c) L=10, d) L=15, e) L=30

Level values are: 0.0 at lower wall, 1.0 at upper wall, 0.1 increments.

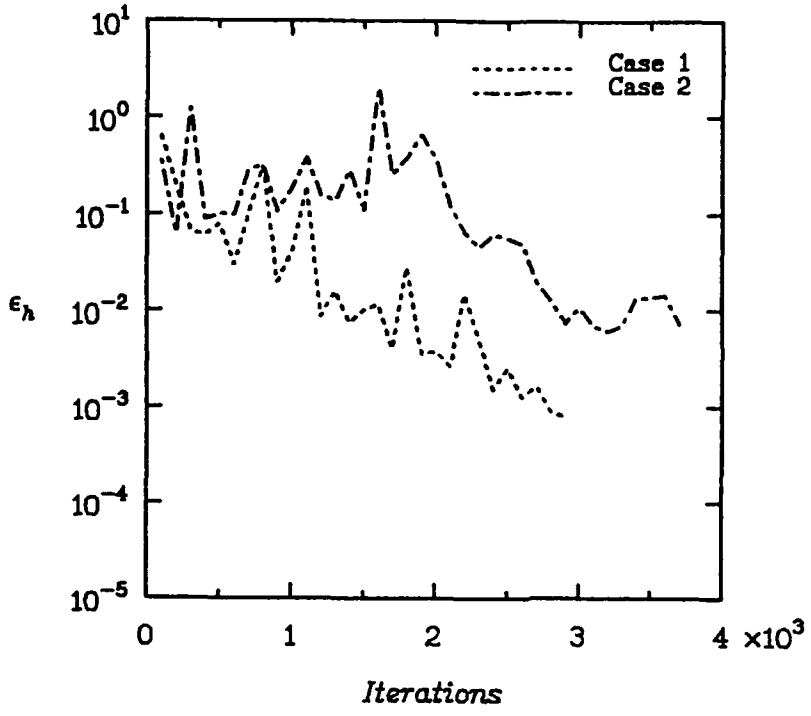

Figure 10. Convergence error for model problems.

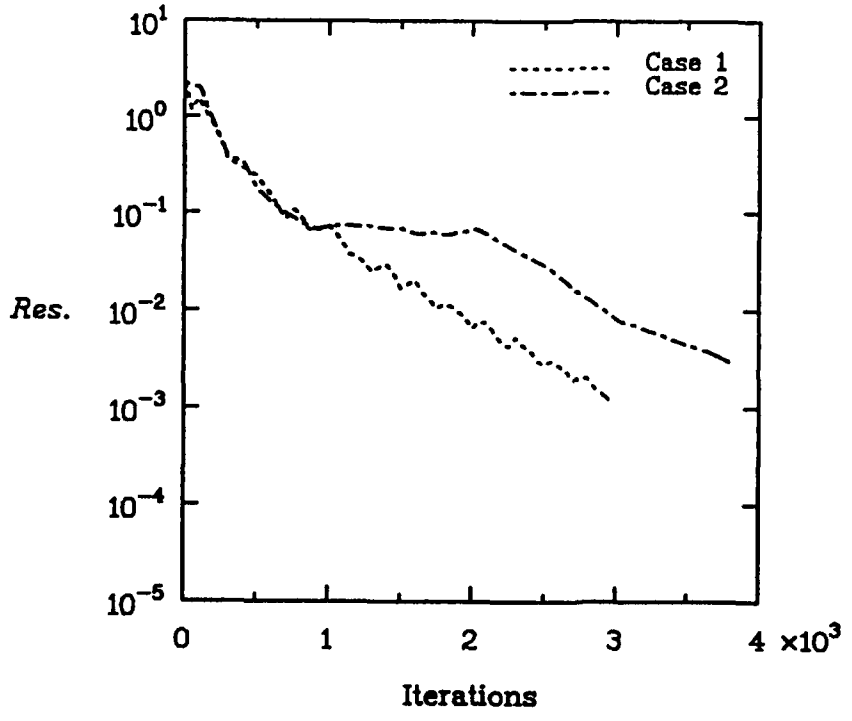

Figure 11. L2–Norm of residuals of the U mom., V mom., and continuity equations for model problems.

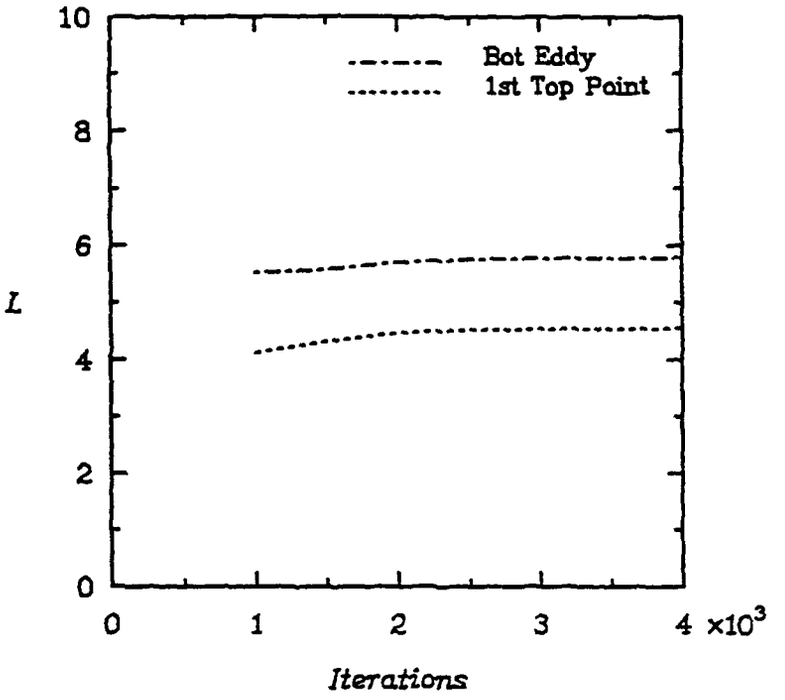

Figure 12. Recirculation zone lengths, case 1.

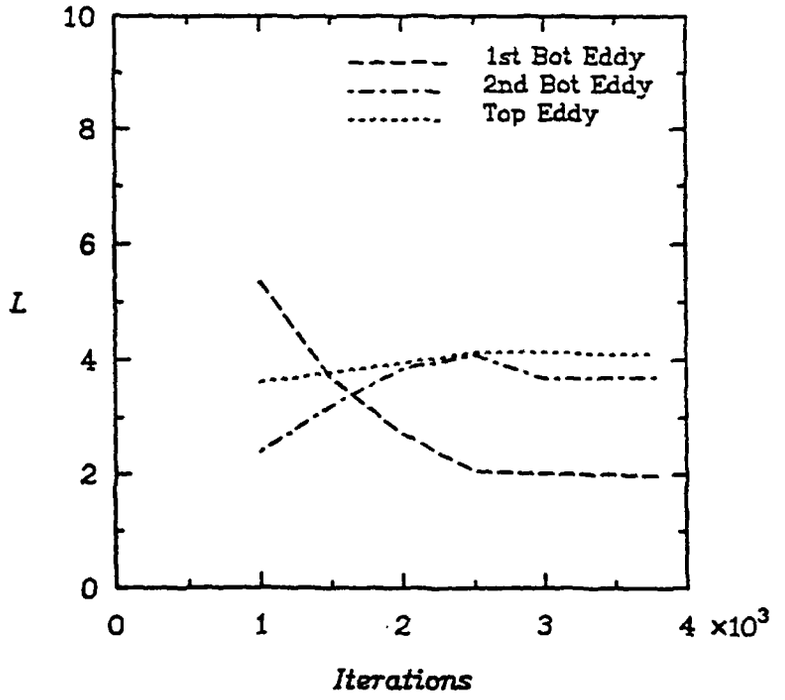

Figure 13. Recirculation zone lengths, case 2.

REPORT DOCUMENTATION PAGE

Form Approved
OMB No 0704-0188

1. AGENCY USE ONLY (Leave blank)	2. REPORT DATE	3. REPORT TYPE AND DATES COVERED
	December 1992	Contractor Report

4. TITLE AND SUBTITLE
ESTIMATING UNCERTAINTY IN COMPUTATIONS OF TWO-DIMENSIONAL SEPARATED FLOWS

5. FUNDING NUMBERS
C NAS1-18605
C NAS1-19480

WU 505-90-52-01

6. AUTHOR(S)
A. O. Demuren
R. V. Wilson

7. PERFORMING ORGANIZATION NAME(S) AND ADDRESS(ES)
Institute for Computer Applications in Science and Engineering
Mail Stop 132C, NASA Langley Research Center
Hampton, VA 23681-0001

8. PERFORMING ORGANIZATION REPORT NUMBER
ICASE Report No. 92-69

9. SPONSORING/MONITORING AGENCY NAME(S) AND ADDRESS(ES)
National Aeronautics and Space Administration
Langley Research Center
Hampton, VA 23681-0001

10. SPONSORING/MONITORING AGENCY REPORT NUMBER
NASA CR-189743
ICASE Report No. 92-69

11. SUPPLEMENTARY NOTES
Langley Technical Monitor: Michael F. Card
Final Report
Submitted to ASME, Journal of Fluids Engineering

12a. DISTRIBUTION/AVAILABILITY STATEMENT
Unclassified - Unlimited

Subject Category 34

12b. DISTRIBUTION CODE

13. ABSTRACT *(Maximum 200 words)*

The present paper investigates sources of uncertainties in two-dimensional flow computations and presents methods for estimating them. Two sample problems are used for illustration. The following categories are explored in detail: i.) Uncertainty due to truncation error in numerical schemes; ii.) Uncertainty due to discretization error; iii.) Uncertainty due to outflow boundary conditions; iv.) Uncertainty due to incomplete iterative convergence; v.) Uncertainty due to computational grid aspect ratio. The error estimates are based on requirements for internal consistencies in computed results. Therefore, they provide better judgement of the numerical solution integrity than comparisons to experimental data or "benchmark" solutions whose reliability may sometimes be questionable. Ideally, both approaches should be employed. New results are presented on the optimum grid-cell aspect ratio for computational accuracy and efficiency.

14. SUBJECT TERMS	15. NUMBER OF PAGES
numerical accuracy; truncation error; discretization error	31
	16. PRICE CODE A03

17. SECURITY CLASSIFICATION OF REPORT	18. SECURITY CLASSIFICATION OF THIS PAGE	19. SECURITY CLASSIFICATION OF ABSTRACT	20. LIMITATION OF ABSTRACT
Unclassified	Unclassified		

National Aeronautics and
Space Administration
Code JTT
Washington, D.C.
20546-0001

Official Business

Penalty for Private Use, $300

BULK RATE
POSTAGE & FEES PAID
NASA
Permit No. G-27

NASA

POSTMASTER: If Undeliverable (Section 158 Postal Manual) Do Not Return